

# UniHetero: Could Generation Enhance Understanding for Vision-Language-Model at Large Data Scale?

Fengjiao Chen\* Minhao Jing Weitao Lu Yan Feng Xiaoyu Li Xuezhi Cao  
Meituan, Beijing, China.

## ABSTRACT

**Takeaway 1: Generation can improve understanding, but Only if you generate Semantics, Not Pixels** A common assumption in unified vision-language models is that adding generation will naturally strengthen understanding. However, this is not always true at scale. At 200M+ pretraining samples, generation helps understanding only when it operates at the semantic level, i.e. when the model learns to autoregress high-level visual representations inside the LLM. Once pixel-level objectives (e.g., diffusion losses) directly interfere with the LLM, understanding performance often degrades.

**Takeaway 2: Generation reveals a superior Data Scaling trend and higher Data Utilization.** Unified generation-understanding demonstrates a superior scaling trend compared to understanding alone, revealing a more effective way to learn vision-only knowledge directive from vision modality rather than captioning to text.

**Takeaway 3: Autoregression on Input Embedding is effective to capture visual details.** Compared to the commonly-used vision encoder, make visual autoregression on input embedding shows less cumulative error and is modality independent, which can be extend to all modalities. The learned semantic representations capture visual information such as objects, locations, shapes, and colors; further enable pixel-level image generation.

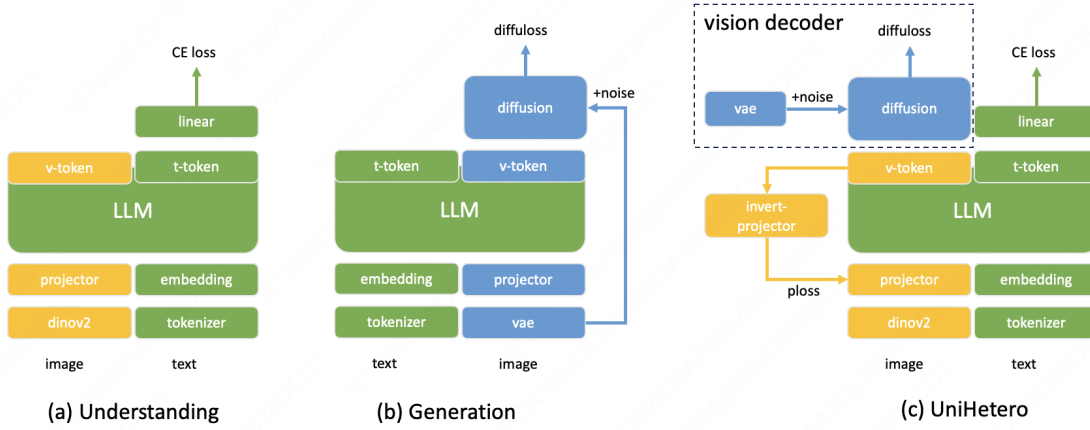


Figure 1: The unified vision language model structure UniHetero, which enables autoregression on semantic representation in LLM layer and transforms the pixel-level representation in modality related decoder structure.

\*Most of the work has been done before 2025.3. Please feel free to contact chenfengjiao02@meituan.com for detailed discussion or cooperation.

## Contents

<b>1</b>	<b>Introduction</b>	<b>3</b>
<b>2</b>	<b>Related Work</b>	<b>3</b>
2.1	Unified Vision Language Models . . . . .	3
2.2	Understanding Enhancement Challenge . . . . .	4
<b>3</b>	<b>Methodology</b>	<b>4</b>
3.1	Model Structure . . . . .	4
3.2	Training Details . . . . .	5
<b>4</b>	<b>Experiment</b>	<b>5</b>
4.1	Generation Enhances Understanding . . . . .	5
4.2	Module Selection Analysis . . . . .	6
4.3	Visualize Semantic Representation . . . . .	8
4.4	Visualize Pixel-Level Representation . . . . .	8
<b>5</b>	<b>Conclusion</b>	<b>8</b>
<b>A</b>	<b>Generation Improvement on Pretraining Stage</b>	<b>12</b>
<b>B</b>	<b>Generation Improvement on Inference Stage</b>	<b>12</b>

## 1 Introduction

With the rapid advancement of multimodal large models in visual understanding and visual generation, unified vision models have emerged as a promising trend for enhancing intelligence levels.

Why are unified models considered favorable? From a model architecture perspective, visual generation structures are increasingly converging with visual understanding structures, with the core architecture predominantly being Transformer-based. Regarding the introduction of conditioning mechanisms, where differences are more pronounced, visual generation models are progressively simplifying, shifting from architecture-driven to data-driven approaches, particularly those capable of supporting multi-image or mixed image-text references. More importantly, from a data standpoint, the integration of tasks leads to an increase in the scale of utilizable data and improves data utilization efficiency under the same data scale.

In unified vision models, by integrating understanding tasks and generation tasks, it is "expected" that generation and understanding mutually reinforce each other, demonstrating a broader range of task formats and higher task performance. The term "expected" is used because the mutual enhancement between understanding tasks and generation tasks has not yet been fully validated, especially regarding the enhancement of understanding through generation.

Existing studies have validated the positive conclusion of "generation enhances understanding" in small-scale experimental settings [Tong et al., 2024, Wang et al., 2024a]. When the data scale is small, the enhancement brought by the data itself may have a greater impact compared to the task format. However, in large-scale production scenarios (with training data exceeding 100M), the effect of generation tasks on understanding tasks is often negative [Team, 2025, Wang et al., 2024b]. Several works [Wu et al., 2024, Ma et al., 2025a] discuss one of the reasons for the difficulty in integrating the two tasks: visual encoding differences. Understanding tasks require high-level semantic representations, while generation tasks require low-level texture representations. The disparity between these representations makes it challenging for existing visual encodings to accommodate both simultaneously. Improvements [Ma et al., 2025a] attempt to fuse these two representations into a unified visual encoder, which shifts the difficulty from the LLM to the encoder which is challenging to solve as well.

To determine whether generation tasks can enhance understanding tasks, it is first essential to validate this in large-scale settings (>100M). In this work, we propose a concise autoregressive model with continuous representation and conduct a series of ablation experiments that verifies "generation enhances understanding" over 200M samples with better data-scale manner. Main contributions

- Demonstrates that generation enhances understanding on over 200M samples by relying on visual semantic representations rather than pixel-level representations.
- Introduces UniHetero, a concise autoregressive model with continuous representations that leverages existing modules to highlight the potential for improved data utilization efficiency in mainstream VLMs.
- Shows that performing autoregression directly on input embeddings is an effective strategy for modeling fine-grained visual details.

## 2 Related Work

### 2.1 Unified Vision Language Models

Vision-language large models are moving toward the unification of visual understanding and visual generation tasks. Existing unified vision models can be structurally categorized into end-to-end architectures and concatenated architectures. In end-to-end architectures, both understanding and generation tasks use the same visual encoder to feed visual information into the LLM backbone. The LLM's parameters adapt to emphasize different tasks depending on the data, thereby achieving comprehensive task fusion [Team, 2025, Wang et al., 2024b, Tong et al., 2024, Ge et al., 2025]. In concatenated architectures, distinct visual encoders are used for understanding and generation tasks to feed visual information into the LLM backbone. The LLM's parameters are explicitly partitioned by task, which prevents performance deterioration on individual tasks, but this design comes at the expense of limiting the possibility of task fusion [Wu et al., 2024, Deng et al., 2025]. Additionally, there are unified models optimized specifically for generation tasks, aiming to enhance generation through understanding without preserving the performance of understanding tasks [Xiao et al., 2024, Tian et al., 2025, Zhou et al., 2024].

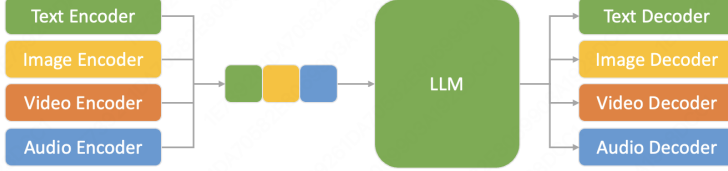


Figure 2: The ideal structure of multimodal large language model.

## 2.2 Understanding Enhancement Challenge

Existing work has validated that understanding enhances generation [Tian et al., 2025, Xiao et al., 2024], but there is a lack of effective verification for generation enhancing understanding, especially under large-scale data pretraining. MetaMorph [Tong et al., 2024], with a sample size of 1M and training only during the SFT stage, demonstrated that as generation data increases, the metrics for understanding tasks show an upward trend. ROSS [Wang et al., 2024a], pretrained on less than 1M samples, concluded through ablation studies that generation data enhances understanding tasks. When the data scale is small, the impact of the data itself on improvement is greater than the task format. However, in large-scale production scenarios (training data volume greater than 100M), the effect of generation tasks on understanding tasks is mostly negative [Team, 2025, Wang et al., 2024b]. Prior studies [Wu et al., 2024, Ma et al., 2025a] point out that a key challenge in unifying these two tasks lies in their differing visual encodings: understanding tasks depend on high-level semantic features, whereas generation tasks require low-level texture details. This mismatch in required representations makes it difficult for current visual encoders to effectively support both types of tasks at once. UniTok [Ma et al., 2025a] attempted to fuse these two representations by enhancing representational capabilities through multi-level codebooks, validating that generation can enhance understanding under discrete encoding with a sample size of 30M.

Leading visual models in understanding primarily use continuous encoding, whereas unified visual encoders mainly rely on discrete encoding. By distilling existing continuous encoders to obtain semantic representations, they can approximate but hardly surpass them. At the same time, unifying visual representations is inherently challenging, effectively shifting the task fusion problem onto the visual encoder. To further explore the improvement of understanding effects through the enhancement of generation tasks based on existing visual understanding models, this work utilizes existing continuous encoders to construct a concise model structure, validating a better data-scale trend under large-scale pretraining.

## 3 Methodology

### 3.1 Model Structure

To investigate the impact of generation tasks on understanding tasks, we propose integrating generation tasks into a visual understanding model while maintaining a concise architecture. This approach aims to preserve visual understanding capabilities while obtaining a multimodal autoregressive model. To mitigate conflicts among representations across different dimensions (in Section 2.2), we intend to fuse multimodal semantic representations inside the LLM and perform modality-specific generation through dedicated "decoders" for each modality, as shown in Figure 2.

Based on the aforementioned considerations, we adopt the model architecture illustrated in Figure 1. To better preserve comprehension capabilities, unlike [Team, 2025, Wang et al., 2024b], we employ continuous encoding to represent visual information, where VAE [Li et al., 2024] represents visual generative representations (noted as pixel feature), and DINOv2 [Oquab et al., 2024] represents visual understanding representations (noted as semantic feature). At the LLM layer, only DINOv2 is used alongside text to perform multimodal auto-regression in the semantic dimension. In the vision decoder component, the image tokens output by the LLM serve as conditional inputs to the diffusion structure, which completes the details, decodes the image VAE features, and ultimately yields pixel-level images.

Consider the visual token with semantic representation  $x^s \in \mathbb{R}^{ds}$  and pixel-level representation  $x^p \in \mathbb{R}^{dp}$ , which denotes the ground-truth token to be predicted. The LLM takes the aligned vector  $e \in \mathbb{R}^D$  from the visual projector and generates the last hidden states  $z \in \mathbb{R}^D$  at that same position. For semantic autoregression, we have Equation 1, which is also used in Seed-X [Ge et al., 2025] and MetaMorph [Tong et al., 2024].

$$\begin{aligned} \mathcal{P}(x_i^s \mid x_{<i}^s) &= \mathcal{P}(x_i^s \mid z_i) \mathcal{P}(z_i \mid x_{<i}^s) \\ &= \mathcal{P}(x_i^s \mid z_i) \mathcal{P}(z_i \mid e_{<i}) \mathcal{P}(e_{<i} \mid x_{<i}^s) \end{aligned} \quad (1)$$

Since the transformation from  $e$  to  $z$  reduces cumulative error,  $z$  and  $e$  have the same dimension, which is easier to learn. Therefore, we model the semantic autoregression on the input embedding  $e$  of LLM in Equation. 2.

$$\mathcal{P}(e_i | e_{<i}) = \mathcal{P}(\hat{e}_i | z_i) \mathcal{P}(z_i | e_{<i}) \quad (2)$$

In this manner, all modalities can be treated within the same autoregressive framework, because  $\mathcal{P}(z_i | e_{<i})$  does not depend on the modality. For  $\mathcal{P}(\hat{e}_i | z_i)$ , it is determined solely by whether the variable is discrete or continuous, rather than by the modality itself.

Then the loss to fit semantic representation uses cosine similarity which shows better performances. More module selection experiments are shown in Section. 4.2.

$$\mathcal{L}_{\text{ploss}} = -\text{cosine}(e_i, \mathbb{E}_{P(\hat{e}_i | e_{<i})} [\hat{e}_i]) \quad (3)$$

And the loss to fit pixel-level representation is

$$\mathcal{L}_{\text{diffuloss}} = \mathbb{E}_{\varepsilon, t} \left[ \|\varepsilon - \varepsilon_\theta(x_t^p | t, z)\|^2 \right] \quad (4)$$

Finally, we have the overall loss as

$$\mathcal{L} = \mathcal{L}_{\text{text}} + \alpha \mathcal{L}_{\text{ploss}} + \beta \mathcal{L}_{\text{diffuloss}} \quad (5)$$

where  $\alpha$  and  $\beta$  are hyper-parameters to adjust the weight of loss.

### 3.2 Training Details

The training process consists of only two stages: pretraining and finetuning. The primary focus is on observing the effects of pretraining, while finetuning is employed solely to evaluate end-to-end performance metrics.

For pretraining, we employ an internal corpus of 80 million image–text aligned pairs tailored for image understanding, running for 3 epochs to yield 240 million training instances in total. Training batch size is 64 and the iteration amount is 37.5K. Throughout training, images are randomly positioned either before or after the text, with the latter arrangement treated as image generation data. Finetuning is then performed on a small internal dataset to initially elicit the model’s capabilities and support experimental evaluation.

We employ Llama2-7B [Touvron et al., 2023] as the LLM backbone and adopt the training configurations from Chameleon [Team, 2025] to facilitate modality fusion, including techniques such as qknorm and zloss. For image representations, semantic features are encoded using DINOv2-large [Oquab et al., 2024], while pixel-level features are encoded from MAR-KL16 [Li et al., 2024]. Both vision encoders are frozen during training to minimize confounding factors. The semantic features are integrated into the LLM via full-attention mechanisms, with masking probabilities sampled from a Gaussian Distribution (mean = 0.7, detailed in Section 3.3.2). As for vision decoder, we follow the similar way in MAR [Li et al., 2024] for training and inference, where the pixel-level features are decoded using flow matching.

To balance the magnitude of losses across different modules, the weighting coefficients are set as  $\alpha = 10$  and  $\beta = 10$ .

## 4 Experiment

The experiments are designed to investigate: (1) whether generative modeling enhances understanding; (2) the semantic content encoded in visual representations; and (3) the capability of heterogeneous representations to synthesize images.

### 4.1 Generation Enhances Understanding

Under the UniHetero model, we analyze whether "generation enhances understanding" through ablation of the image generation loss. The experiment settings are shown in the Table. 1. The control group exp1 uses only the text generation loss, while the experimental groups exp2 and exp3, adds two types of image generation losses on top of the control group respectively. In terms of implementation, exp2 does not completely remove the diffusion loss but prevents gradients from back propagating to the LLM, thereby reducing the impact on image understanding while retaining image generation capabilities.

To observe the data-scale trending quantitatively, we use a linear regression to fit the performance in Equation 6.

$$y = an + b \quad (6)$$

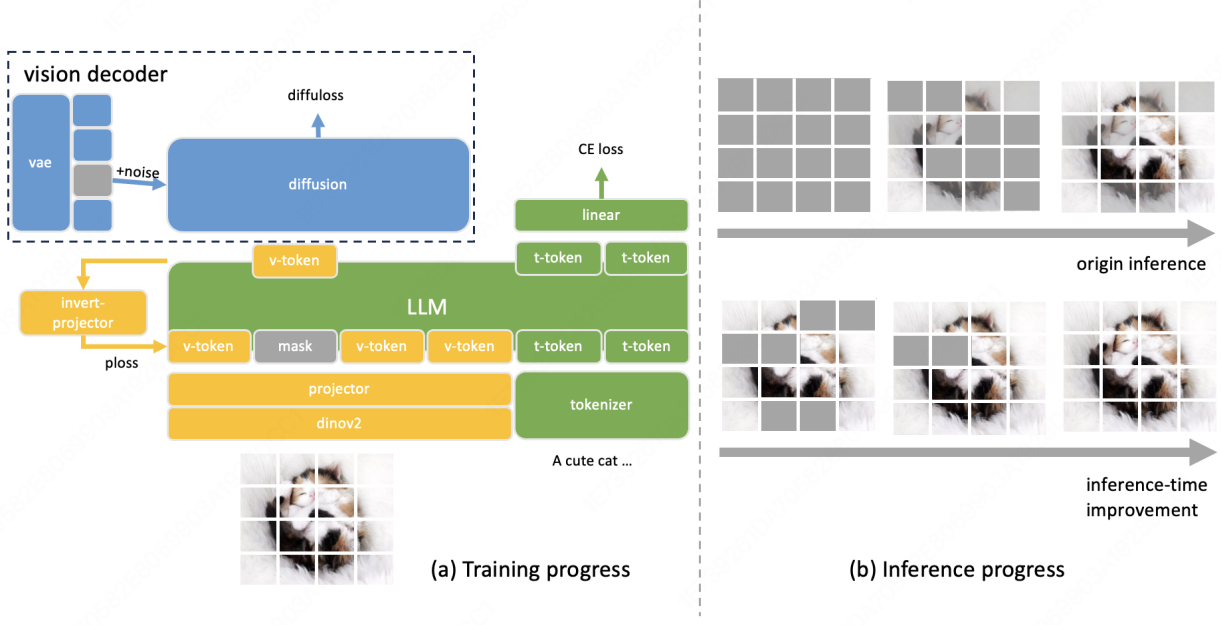


Figure 3: Illustration of training and inference progress in UniHetero. (a) shows the training progress with autoregression on input embedding rather than vision encoder and gaussian distribution for mask\_rate scheduler. (b) shows the inference progress where a inference-time improvement is proposed to refine the pixel-level generation without influence understanding ability.

ID	Method	diffuloss	ploss	MMBench	MMBench( $a$ )	SeedBench	SeedBench( $a$ )
exp1	baseline	0	0	0.6357	$-4 \times 10^{-4}$	0.6668	$8 \times 10^{-4}$
exp2	+ploss	0	1	<b>0.6460</b>	$66 \times 10^{-4}$	<b>0.6696</b>	$26 \times 10^{-4}$
exp3	+diffuloss	1	1	0.6168	$62 \times 10^{-4}$	0.6456	$7 \times 10^{-4}$
exp4	+warmup	1	1	0.6271	$30 \times 10^{-4}$	0.6585	$7 \times 10^{-4}$

Table 1: Ablation performances of UniHetero on various image generation strategies at more than 200M data-scale.

where  $a$  indicates the data-scale trending,  $n$  is the amount of data samples,  $y$  is the evaluation metric.

The experimental results in Figure. 4 reveals that using only ploss (i.e. UniHetero\_ploss) shows a favorable scaling trend in understanding performances, eventually surpassing other model settings in later training stages, validating that generation enhances understanding.

Furthermore, introducing diffuLoss causes a decline in understanding performance and weakens the scaling trend, as illustrated in Figure 5. A conflict between semantic representation and pixel-level representation emerges, which is consistent with findings reported in previous studies [Chen et al., 2025, Wu et al., 2024]. It seems that the vision decoder module accomplishes the representation transformation through leveraging LLM rather than by itself.

Could the transformation decrease the dependence on LLMs? To explore this further, an additional experiment (denoted "+warmup") was performed by increasing the size of the diffusion structure and applying a warm-up phase to the model parameters. In practice, we adopt the pretrained mar-base-f32 model [Li et al., 2024], which is concise than Stable Diffusion [Esser et al., 2024] and shows remarkable class-condition generation performance. The experimental findings show a substantial boost in performance on understanding tasks, suggesting that image generation can potentially be realized without relying on LLM-based compensation or intricate architectures.

## 4.2 Module Selection Analysis

The selection of the invert-projector architecture and loss function was rapidly validated through small-scale experiments.

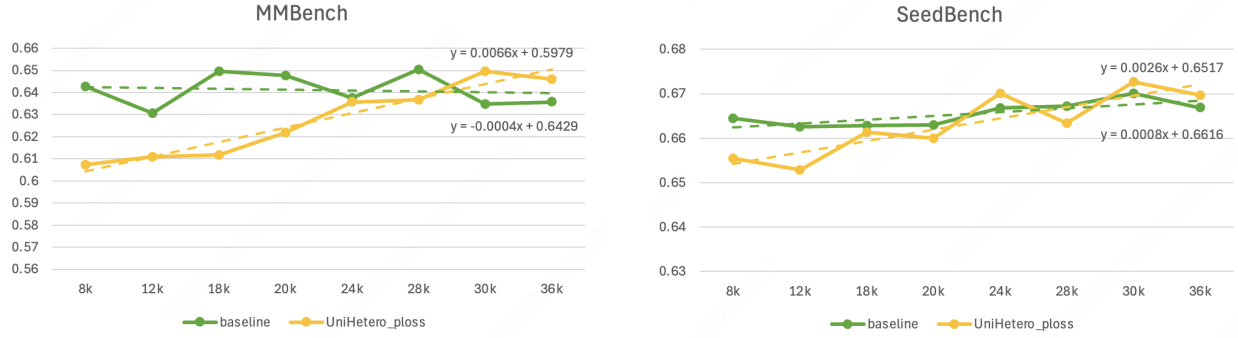


Figure 4: Performance of UniHetero with ploss using over 200M data samples. The x-axis represents the training steps. The dashed lines show the linear regression fit for the data scaling law.

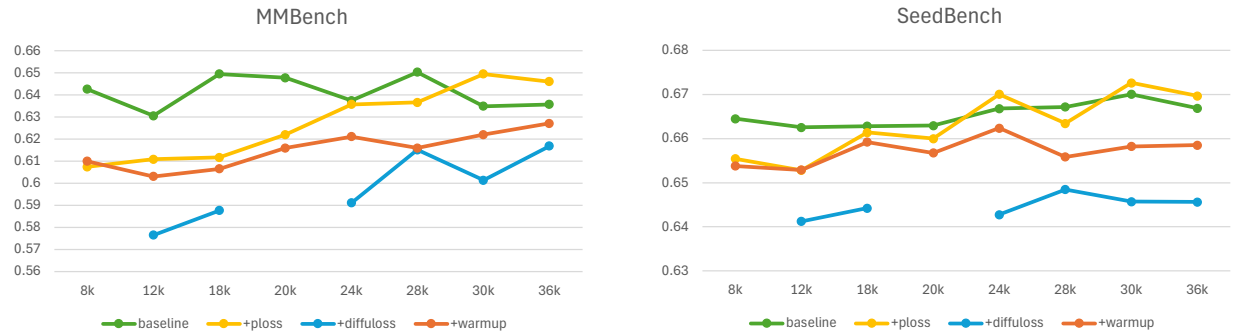


Figure 5: Ablation results for different vision generation configurations. “+ploss” indicates UniHetero using only ploss. “+diffuloss” refers to UniHetero using both ploss and diffuloss. “+warmup” corresponds to UniHetero employing ploss, diffuloss, and a warmed-up diffusion module.

Method	Loss	Invert-Projector	Target	MMBench	SeedBench
diffu-mse	MSE Loss	Diffusion(MAR-base)	Vision Encoder	-	-
mlp-mse	MSE Loss	1x MLP	Vision Encoder	-	-
mlp-cos	Cosine Loss	1x MLP	Vision Encoder	0.5833	0.6189
norm-3-mlp-cos	Cosine Loss	3x MLP+norm (MetaMorph)	Vision Encoder	0.5773	0.6502
ema-mlp-llm-cos	Cosine Loss	1xMLP+momentum	Input Embedding	0.6168	0.6456

Table 2: Different module settings on loss, target and the structure of invert-projector.

As shown in Table. 2, we first compare mlp-cos, diffu-mse and mlp-mse on caption tasks for a quick observation. Results show that mlp-cos performs the best, which aligns with conclusions from existing studies [Tong et al., 2024, Wang et al., 2024a, Ge et al., 2025].

Next, we conduct finer experiments with end-to-end metrics (MMBench [Liu et al., 2024] and SeedBench [Li et al., 2023]) to select the module setting. Experiments indicate that fitting the input to the LLM layer yields superior results compared to fitting the output of the Vision Encoder. Specifically, the ranking observed is: ema-mlp-llm-cos > norm-3-mlp-cos > mlp-cos. This confirms the hypothesis in Equation. 2, namely that performing autoregression on the LLM input embeddings results in lower cumulative error and improved modality adaptation. To achieve a similar level of performance, the commonly adopted fitting vision encoder (Equation. 1) requires a larger number of parameters under the norm-3-mlp-cos configuration.

Furthermore, we also examine the effectiveness of pixel-level representations by overfitting on single image. The generation results, as shown in the Figure.6, demonstrate that heterogeneous representations possess image generation capabilities and autoregression on input embedding is efficient to capture visual details.

Finally, we mention that when fitting the LLM input, it is important to stabilize gradients via momentum-based updates or potentially by truncating gradient flow.

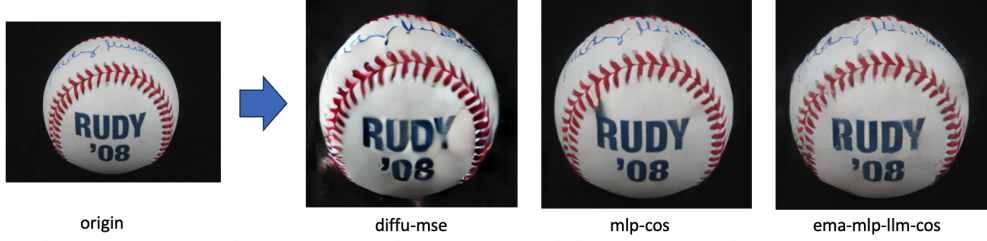


Figure 6: Visualization of overfitting generation on one image with various module setting (in Table. 2).

### 4.3 Visualize Semantic Representation

In the previous section’s experiments, we observed that through autoregressive modeling of visual-semantic representations, generation can be verified to improve understanding on a large-scale dataset. Then, do visual-semantic representations actually capture? To investigate this, we now turn to a qualitative analysis.

Since visual-semantic representations cannot directly generate images, we adopt an indirect approach: first generate a visual representation from text, then use this representation to regenerate text, and examine whether the original textual information is preserved.

As shown in Figure.7, the first column displays the original images, the second column presents the captions of these images, and the third column shows the text regenerated from the visual representations generated based on these captions. Since this exploration was conducted directly after pretraining, the model’s ability to follow instructions was not optimal. Therefore, a finetuned version is added in the fourth column. It can be observed that most image details, such as color, shape, and spatial position, are preserved through the semantic representations, though some recognition errors still exist.

### 4.4 Visualize Pixel-Level Representation

Although overfitting on single image works well in the Figure.6, the quality of general image generation remains relatively low. While image generation quality is not the primary focus of this work, we have also explored potential directions for optimization.

We identify the discrepancy between training and inference as a major factor affecting generation performance. To mitigate this gap, we introduce an improved mask-rate scheduler for the training stage (Appendix A) and an inference-time scaling strategy for the inference stage (Appendix B). Both techniques yield performance gains, highlighting the promise of pixel-level image generation.

## 5 Conclusion

This work constructs UniHetero, a unified generation-understanding model under continuous encoding, which features a concise architecture and straightforward training. The study shows that the unified model attains a better data scaling pattern than models focused solely on image understanding, validating under large-scale pretraining that generation facilitates understanding. Preserving the LLM layer for semantic representation fusion may be key to learning multimodal knowledge.

The image semantic representations learn information such as objects, locations, shapes, and colors; the low-dimensional image representations enable pixel-level image generation. Image generation performance is further improved through pretraining data, masked sampling, and multi-round inference optimization, which showing potential for inference-time scaling.

## Limitations

In the future, we will continue our investigation along two main directions.

**Improve Pixel-level Generation.** While generation helps with semantic understanding, the model’s pixel-level visual synthesis remains weak. Potential improvements include using a larger vision decoder or employing a more effective

txt	txt->img->txt	txt->img->txt.sft
	一只灰白相间的猫躺在木地板上，正在玩耍。猫的身体呈侧卧姿势，前爪伸展开来，似乎在抓或拍打一个色彩鲜艳的毛线球。毛线球上有紫色、粉色和蓝色的条纹，看起来像一个猫玩具。猫的尾巴卷曲着，头部微微抬起，似乎全神贯注于玩耍。阳光从画面左侧照射进来，在木地板上投下柔和的阴影，营造出温馨的家庭氛围。	a cat playing with a ball on the floor.
	一只小猫蜷缩在柔软的白色毛毯上，正在安静地睡觉。它的身体呈卷曲状，前爪轻轻地搭在肚子上，后腿弯曲，尾巴环绕着身体。这只小猫的毛色是典型的三花猫，有着白色、橙色和黑色的斑块。它的眼睛紧闭，粉红色的鼻子显得十分可爱。整个场景传达出一种宁静和温馨的感觉。	A small orange kitten is sleeping on a red blanket.
(a) Visualize semantic representations on animals.		
	This image captures a serene lakeside scene. The main subject is a body of water, possibly a lake or a river, with a canoe gently floating on its surface. The water reflects the sky above, which is filled with large, puffy white clouds. The canoe is surrounded by lush, green trees that add to the sense of peace and solitude. The photographic style is realistic, with an emphasis on detail and texture. The photographic techniques used include a wide-angle lens, which allows for a broad view of the scene, and a shallow depth of field, which places the canoe in sharp focus while the background blurs subtly. The image conveys a sense of calm and natural beauty.	The image depicts a serene landscape featuring a calm lake surrounded by lush greenery. The sky above is a vibrant blue, dotted with fluffy white clouds that are illuminated by the sun's rays, creating a radiant effect. The water reflects the sky and the surrounding trees, adding to the tranquility of the scene. The trees on the left side of the image are dense and appear to be a mix of deciduous and coniferous varieties, suggesting a temperate climate. The overall atmosphere of the image is peaceful and idyllic, evoking a sense of calm and natural beauty.
(b) Visualize semantic representations on nature scenes.		
	This image showcases a modern living room area, featuring a long wooden dining table accompanied by multiple matching chairs. The room is further accessorized with a large white screen and a stone wall, all under a stone ceiling. The photographic style suggests a realism approach, with an emphasis on detail and textures. The wide-angle lens used captures the entire breadth of the room, providing a sense of its size and layout.	The image depicts a modern dining room with a long wooden table and chairs. The room is illuminated by a warm, reddish-orange light, creating a cozy and inviting atmosphere. The table is surrounded by several chairs, each with a unique design. The room is spacious, with a large window providing natural light. The ceiling is painted in a bright red color, adding to the room's modern aesthetic.
	three white pillows with blue crosses on them	Two white pillows with blue crosses on them.
(c) Visualize semantic representations badcases.		

Figure 7: Visualize semantic representations on different scenarios.

warm-up schedule, adopting training strategies that mitigate negative side effects, and applying inference-time scaling techniques.

**Expand Semantic Representation Advantage.** The potential of learning from visual information remains insufficiently explored. Possible directions include acquiring physical knowledge from video data, generating semantic images as a form of visual CoT, and extracting visual knowledge without relying on aligned captions. Meanwhile, determining how to evaluate and verify what has been learned from such semantic representations is both essential and challenging.

## Acknowledgement

We hereby express our appreciation to the LongCat Team EVA Committee for their valuable assistance, guidance, and suggestions throughout the course of this work.

## References

Shengbang Tong, David Fan, Jiachen Zhu, Yunyang Xiong, Xinlei Chen, Koustuv Sinha, Michael Rabbat, Yann LeCun, Saining Xie, and Zhuang Liu. Metamorph: Multimodal understanding and generation via instruction tuning, 2024. URL <https://arxiv.org/abs/2412.14164>.

Haochen Wang, Anlin Zheng, Yucheng Zhao, Tiancai Wang, Zheng Ge, Xiangyu Zhang, and Zhaoxiang Zhang. Reconstructive visual instruction tuning, 2024a. URL <https://arxiv.org/abs/2410.09575>.

Chameleon Team. Chameleon: Mixed-modal early-fusion foundation models, 2025. URL <https://arxiv.org/abs/2405.09818>.

Xinlong Wang, Xiaosong Zhang, Zhengxiong Luo, Quan Sun, Yufeng Cui, Jinsheng Wang, Fan Zhang, Yueze Wang, Zhen Li, Qiying Yu, Yingli Zhao, Yulong Ao, Xuebin Min, Tao Li, Boya Wu, Bo Zhao, Bowen Zhang, Liangdong Wang, Guang Liu, Zheqi He, Xi Yang, Jingjing Liu, Yonghua Lin, Tiejun Huang, and Zhongyuan Wang. Emu3: Next-token prediction is all you need, 2024b. URL <https://arxiv.org/abs/2409.18869>.

Chengyue Wu, Xiaokang Chen, Zhiyu Wu, Yiyang Ma, Xingchao Liu, Zizheng Pan, Wen Liu, Zhenda Xie, Xingkai Yu, Chong Ruan, and Ping Luo. Janus: Decoupling visual encoding for unified multimodal understanding and generation, 2024. URL <https://arxiv.org/abs/2410.13848>.

Chuofan Ma, Yi Jiang, Junfeng Wu, Jihan Yang, Xin Yu, Zehuan Yuan, Bingyue Peng, and Xiaojuan Qi. Unitok: A unified tokenizer for visual generation and understanding, 2025a. URL <https://arxiv.org/abs/2502.20321>.

Yuying Ge, Sijie Zhao, Jinguo Zhu, Yixiao Ge, Kun Yi, Lin Song, Chen Li, Xiaohan Ding, and Ying Shan. Seed-x: Multimodal models with unified multi-granularity comprehension and generation, 2025. URL <https://arxiv.org/abs/2404.14396>.

Chaorui Deng, Deyao Zhu, Kunchang Li, Chenhui Gou, Feng Li, Zeyu Wang, Shu Zhong, Weihao Yu, Xiaonan Nie, Ziang Song, Guang Shi, and Haoqi Fan. Emerging properties in unified multimodal pretraining. *arXiv preprint arXiv:2505.14683*, 2025.

Shitao Xiao, Yueze Wang, Junjie Zhou, Huaying Yuan, Xingrun Xing, Ruiran Yan, Shuting Wang, Tiejun Huang, and Zheng Liu. Omnigen: Unified image generation. *arXiv preprint arXiv:2409.11340*, 2024.

Rui Tian, Mingfei Gao, Mingze Xu, Jiaming Hu, Jiasen Lu, Zuxuan Wu, Yinfei Yang, and Afshin Dehghan. Unigen: Enhanced training & test-time strategies for unified multimodal understanding and generation, 2025. URL <https://arxiv.org/abs/2505.14682>.

Chunting Zhou, Lili Yu, Arun Babu, Kushal Tirumala, Michihiro Yasunaga, Leonid Shamis, Jacob Kahn, Xuezhe Ma, Luke Zettlemoyer, and Omer Levy. Transfusion: Predict the next token and diffuse images with one multi-modal model, 2024. URL <https://arxiv.org/abs/2408.11039>.

Tianhong Li, Yonglong Tian, He Li, Mingyang Deng, and Kaiming He. Autoregressive image generation without vector quantization, 2024. URL <https://arxiv.org/abs/2406.11838>.

Maxime Oquab, Timothée Darcet, Théo Moutakanni, Huy Vo, Marc Szafraniec, Vasil Khalidov, Pierre Fernandez, Daniel Haziza, Francisco Massa, Alaaeldin El-Nouby, Mahmoud Assran, Nicolas Ballas, Wojciech Galuba, Russell Howes, Po-Yao Huang, Shang-Wen Li, Ishan Misra, Michael Rabbat, Vasu Sharma, Gabriel Synnaeve, Hu Xu, Hervé Jegou, Julien Mairal, Patrick Labatut, Armand Joulin, and Piotr Bojanowski. Dinov2: Learning robust visual features without supervision, 2024. URL <https://arxiv.org/abs/2304.07193>.

Hugo Touvron, Louis Martin, Kevin Stone, Peter Albert, Amjad Almahairi, Yasmine Babaei, Nikolay Bashlykov, Soumya Batra, Prajjwal Bhargava, Shruti Bhosale, Dan Bikel, Lukas Blecher, Cristian Canton Ferrer, Moya Chen, Guillem Cucurull, David Esiobu, Jude Fernandes, Jeremy Fu, Wenjin Fu, Brian Fuller, Cynthia Gao, Vedanuj Goswami, Naman Goyal, Anthony Hartshorn, Saghar Hosseini, Rui Hou, Hakan Inan, Marcin Kardas, Viktor Kerkez, Madian Khabsa, Isabel Kloumann, Artem Korenev, Punit Singh Koura, Marie-Anne Lachaux, Thibaut Lavril, Jenya Lee, Diana Liskovich, Yinghai Lu, Yuning Mao, Xavier Martinet, Todor Mihaylov, Pushkar Mishra, Igor Molybog, Yixin Nie, Andrew Poulton, Jeremy Reizenstein, Rashi Rungta, Kalyan Saladi, Alan Schelten, Ruan Silva, Eric Michael Smith, Ranjan Subramanian, Xiaoqing Ellen Tan, Binh Tang, Ross Taylor, Adina Williams, Jian Xiang Kuan, Puxin Xu, Zheng Yan, Iliyan Zarov, Yuchen Zhang, Angela Fan, Melanie Kambadur, Sharan Narang, Aurelien Rodriguez, Robert Stojnic, Sergey Edunov, and Thomas Scialom. Llama 2: Open foundation and fine-tuned chat models, 2023. URL <https://arxiv.org/abs/2307.09288>.

Jiuhai Chen, Zhiyang Xu, Xichen Pan, Yushi Hu, Can Qin, Tom Goldstein, Lifu Huang, Tianyi Zhou, Saining Xie, Silvio Savarese, Le Xue, Caiming Xiong, and Ran Xu. Blip3-o: A family of fully open unified multimodal models-architecture, training and dataset, 2025. URL <https://arxiv.org/abs/2505.09568>.

Patrick Esser, Sumith Kulal, Andreas Blattmann, Rahim Entezari, Jonas Müller, Harry Saini, Yam Levi, Dominik Lorenz, Axel Sauer, Frederic Boesel, Dustin Podell, Tim Dockhorn, Zion English, Kyle Lacey, Alex Goodwin, Yannik Marek, and Robin Rombach. Scaling rectified flow transformers for high-resolution image synthesis, 2024. URL <https://arxiv.org/abs/2403.03206>.

Yuan Liu, Haodong Duan, Yuanhan Zhang, Bo Li, Songyang Zhang, Wangbo Zhao, Yike Yuan, Jiaqi Wang, Conghui He, Ziwei Liu, et al. Mmbench: Is your multi-modal model an all-around player? In *European conference on computer vision*, pages 216–233. Springer, 2024.

Bohao Li, Rui Wang, Guangzhi Wang, Yuying Ge, Yixiao Ge, and Ying Shan. Seed-bench: Benchmarking multimodal llms with generative comprehension. *arXiv preprint arXiv:2307.16125*, 2023.

Nanye Ma, Shangyuan Tong, Haolin Jia, Hexiang Hu, Yu-Chuan Su, Mingda Zhang, Xuan Yang, Yandong Li, Tommi Jaakkola, Xuhui Jia, and Saining Xie. Inference-time scaling for diffusion models beyond scaling denoising steps, 2025b. URL <https://arxiv.org/abs/2501.09732>.

Ziyu Guo, Renrui Zhang, Chengzhuo Tong, Zhizheng Zhao, Rui Huang, Haoquan Zhang, Manyuan Zhang, Jiaming Liu, Shanghang Zhang, Peng Gao, Hongsheng Li, and Pheng-Ann Heng. Can we generate images with cot? let's verify and reinforce image generation step by step, 2025. URL <https://arxiv.org/abs/2501.13926>.

## A Generation Improvement on Pretraining Stage

First, the current training data uses reversed image-understanding data as image-generation data without filtering for image quality or adjusting captions accordingly, which is not conducive to image generation quality. Therefore, by incorporating high-quality image generation data, we observed some improvement in image texture and details, but issues such as disharmonious distortions and blurring between tokens still persist.

Considering the consistency between training and inference (the same as MAR inference), the masking probability has a significant impact. A higher masking probability can improve image generation learning but may negatively affect image understanding. Meanwhile, during inference, the masking probability decreases from 1.0 to 0, so the training process needs to expose the model to various masking probabilities. Therefore, we replaced the fixed masking probability in training with Gaussian sampling with a mean of 0.7. As shown in Figure.8, experimental results show a significant improvement in image generation quality.

## B Generation Improvement on Inference Stage

During the inference stage, further consideration is given to the differences between training and inference. During training, it is assumed that unmasked tokens are correct and the average mask rate is around 70%, but this assumption does not hold during inference, especially for the initial steps where prediction starts from 100% masking, making the task more difficult and resulting in lower token quality, which significantly differs from the conditions in training. Therefore, we consider evaluating token generation quality after one round of generation, selectively retaining high-quality tokens, and regenerating low-quality ones until overall quality can no longer be improved. However, this requires training a token-level reward model. As an initial attempt, we randomly select tokens for regeneration, assuming that most generated tokens are of acceptable quality, and regenerate them either in their original order or with random masking.

The experimental results are shown in the Figure.9. For most generated samples, quality improves after one random iteration, with issues such as distortion and blurry details being mitigated. However, there are cases where the original generated image was of good quality but degrades after regeneration, indicating that selective regeneration is still necessary. This aligns with the concept of "inference-time scaling" in the generation field [Ma et al., 2025b, Guo et al., 2025], suggesting that this direction has potential for further exploration.

text	exp4	+high quality data	+gaussian mask rate
一只灰白相间的猫躺在木地板上，正在玩耍。猫的身体呈侧卧姿势，前爪伸展开来，似乎在抓或拍打一个色彩鲜艳的毛线球。毛线球上有紫色、粉色和蓝色的条纹，看起来像是一个猫玩具。猫的尾巴卷曲着，头部微微抬起，似乎全神贯注于玩耍。阳光从画面左侧照射进来，在木地板上投下柔和的阴影，营造出温馨的家庭氛围。			
一只小猫咪蜷缩在柔软的白色毛毯上，正在安静地睡觉。它的身体呈卷曲状，前爪轻轻地搭在肚子上，后腿弯曲，尾巴环绕着身体。这只小猫的毛色是典型的三花猫，有着白色、橙色和黑色的斑块。它的眼睛紧闭，粉红色的鼻子显得十分可爱。整个场景传达出一种宁静和温馨的感觉。			
这张图片展示了一个宁静的湖畔景色。湖水平静，反射着周围树木和天空的影像。湖边长满了绿色的植被，包括一些水生植物。湖对面是一片茂密的针叶林，树木高大，树冠茂密，呈现出深浅不一的绿色。天空中有大量的云彩，但云层之间有蓝天透出，阳光从云层缝隙中照射下来，给整个场景增添了柔和的光线。整体上，这张图片传达了一种宁静、清新的自然氛围。			
A black dog			
A glass of wine			

Figure 8: Visualize the generation improvement on pretraining stage.

text	Inference base	+1turn_order	+1turn_random	+2turn_random	+3turn_random
一只灰白相间的猫躺在木地板上，正在玩耍。猫的身体呈侧卧姿势，前爪伸展开来，似乎在抓或拍打一个色彩鲜艳的毛线球。毛线球上有紫色、粉色和蓝色的条纹，看起来像是一个猫玩具。猫的尾巴卷曲着，头部微微抬起，似乎全神贯注于玩耍。阳光从画面左侧照射进来，在木地板上投下柔和的阴影，营造出温馨的家庭氛围。					
一只小猫咪蜷缩在柔软的白色毛毯上，正在安静地睡觉。它的身体呈卷曲状，前爪轻轻地搭在肚子上，后腿弯曲，尾巴环绕着身体。这只小猫的毛色是典型的三花猫，有着白色、橙色和黑色的斑块。它的眼睛紧闭，粉红色的鼻子显得十分可爱。整个场景传达出一种宁静和温馨的感觉。					
这张图片展示了一个宁静的湖畔景色。湖水平静，反射着周围树木和天空的影像。湖边长满了绿色的植被，包括一些水生植物。湖对面是一片茂密的针叶林，树木高大，树冠茂密，呈现出深浅不一的绿色。天空中有大量的云彩，但云层之间有蓝天透出，阳光从云层缝隙中照射下来，给整个场景增添了柔和的光线。整体上，这张图片传达了一种宁静、清新的自然氛围。					

Figure 9: Visualize the generation improvement on inference stage.